Characteristics of dielectric-band modified single-cell photonic crystal lasers

You-Shin No,[1] Ho-Seok Ee,[1] Soon-Hong Kwon,[1,*] Sun-Kyung Kim,[2] Min-Kyo Seo,[3] Ju-Hyung Kang,[3] Yong-Hee Lee,[3] and Hong-Gyu Park[1,*]

[1]*Department of Physics, Korea University, Seoul 136-701, Korea*
[2]*Advanced Technology Laboratory, LED Division, LG Innotek, Seoul 137-724, Korea*
[3]*Department of Physics, Korea Advanced Institute of Science and Technology, Daejeon 305-701, Korea*
[*]*Corresponding authors: soonhong.kwon@gmail.com, hgpark@korea.ac.kr*

Abstract: We demonstrate new types of dielectric-band photonic crystal lasers in a two-dimensional modified single-cell cavity with enlarged air holes. Finite-difference time-domain simulations performed in real and Fourier spaces show that the dielectric-band cavity modes originating from the first band edge point in the dielectric band have mode patterns that are distinguishable from conventional air-band cavity modes. In our experiment, the observed multimode lasing peaks are identified as the hexapole and the monopole dielectric-band cavity modes through the spectral positions and mode images. The thresholds of these lasers are measured as ~340 μW and ~450 μW, respectively, at room temperature. In addition, using the simulation based on the actual fabricated structures, quality factors and mode volumes are computed as 4900 and 1.09 $(\lambda/n)^3$ for the hexapole mode, and 4300 and 2.27 $(\lambda/n)^3$ for the monopole mode, respectively.

OCIS codes: (230.5298) Photonic crystals; (220.4241) Nanostructure fabrication; (140.5960) Semiconductor lasers; (140.3945) Microcavities; (250.5300) Photonic integrated circuits

References and links

1. Y. Akahane, T. Asano, B.-S. Song and S. Noda, "High-Q photonic nanocavity in a two-dimensional photonic crystal," Nature **425**, 944-947 (2003).
2. B.-S. Song, S. Noda, T. Asano and Y. Akahane, "Ultra-high-Q photonic double-heterostructure nanocavity," Nature Mater. **4**, 207-210 (2005).
3. T. Tanabe, A. Shinya, E. Kuramochi, S. Kondo, H. Taniyama and M. Notomi, "Single point defect photonic crystal nanocavity with ultrahigh quality factor achieved by using hexapole mode," Appl. Phys. Lett. **91**, 021110 (2007).
4. K. Nozaki and T. Baba, "Laser characteristics with ultimate-small modal volume in photonic crystal slab point-shift nanolasers," Appl. Phys. Lett. **88**, 211101 (2006).
5. H.-S. Ee, K.-Y. Jeong, M.-K. Seo, Y.-H. Lee and H.-G. Park, "Ultrasmall square-lattice zero-cell photonic crystal laser," Appl. Phys. Lett. **93**, 011104 (2008).
6. G.-H. Kim, Y.-H. Lee, A. Shinya and M. Notomi, "Coupling of small, low-loss hexapole mode with photonic crystal slab waveguide mode," Opt. Express **12**, 6624-6631 (2004).
7. S.-H. Kwon, T. Sünner, M. Kamp and A. Forchel, "Ultrahigh-Q photonic crystal cavity created by modulating air hole radius of a waveguide," Opt. Express **16**, 4605-4614 (2008).
8. H.-G. Park, C. J. Barrelet, Y. Wu, B. Tian, F. Qian and C. M. Lieber, "A wavelength-selective photonic-crystal waveguide coupled to a nanowire light source," Nature Photonics **2**, 622-626 (2008).
9. T. Tanabe, M. Notomi, S. Mitsugi, A. Shinya and E. Kuramochi, "Fast bistable all-optical switch and memory on a silicon photonic crystal on-chip," Opt. Lett. **30**, 2575-2577 (2005).
10. J. M. Gerard and B. Gayral, "Toward high-efficiency quantum-dot single-photon sources," Proc. SPIE **5361**, 88 (2004).
11. T. Yoshie, A. Scherer, J. Hendrickson, G. Khitrova, H. M. Gibbs, G. Rupper, C. Ell, O. B. Shchekin and D. G. Deppe, "Vacuum Rabi splitting with a single quantum dot in a photonic crystal nanocavity," Nature **432**, 200-203 (2004).
12. J. D. Joannopoulos, S. G. Johnson, J. N. Winn and R. D. Meade, *Photonic Crystals: Molding the Flow of Light* (Princeton University Press, New Jersey, 2008).

#105071 - $15.00 USD Received 9 Dec 2008; revised 20 Jan 2009; accepted 21 Jan 2009; published 27 Jan 2009

13. H.-G. Park, S.-H. Kim, S.-H. Kwon, Y.-G. Ju, J.-K. Yang, J.-H. Baek, S.-B. Kim and Y.-H. Lee, "Electrically Driven Single-Cell Photonic Crystal Laser," Science **305**, 1444-1447 (2004).
14. K. Srinivasan and O. Painter, "Momentum space design of high-Q photonic crystal optical cavities," Opt. Express **10**, 670-684 (2002).
15. K. Srinivasan and O. Painter, "Fourier space design of high-Q cavities in standard and compressed hexagonal lattice photonic crystals," Opt. Express **11**, 579-593 (2003).
16. Z. Zhang and M. Qiu, "Compact in-plane channel drop filter design using a single cavity with two degenerate modes in 2D photonic crystal slabs," Opt. Express **13**, 2596-2604 (2005).
17. D. Englund, D. Fattal, E. Waks, G. Solomon, B. Zhang, T. Nakaoka, Y. Arakawa, Y. Yamamoto and J. Vuckovic, "Controlling the Spontaneous Emission Rate of Single Quantum Dots in a Two-Dimensional Photonic Crystal," Phys. Rev. Lett. **95**, 013904 (2005).
18. This single-cell cavity is advantageous to the demonstration of the electrically driven laser by introducing a small central post underneath the cavity.
19. K. Srinivasan, P. E. Barclay and O. Painter, "Fabrication-tolerant high quality factor photonic crystal microcavities," Opt. Express **12**, 1458-1463 (2004).
20. T. Asano, B.-S. Song and S. Noda, "Analysis of the experimental Q factors (~1 million) of photonic crystal nanocavities," Opt. Express **14**, 1996-2002 (2006).
21. S.-H. Kim and Y.-H. Lee, "Symmetry Relations of Two-Dimensional Photonic Crystal Cavity Modes," IEEE J. Quantum Electron. **39**, 1081-1085 (2003).
22. S.-H. Kim, S.-K. Kim and Y.-H. Lee, "Vertical beaming of wavelength-scale photonic crystal resonators," Phys. Rev. B **73**, 235117 (2006).
23. S. G. Johnson, S. Fan, A. Mekis and J. D. Joannopoulos, "Multipole-cancellation mechanism for high-Q cavities in the absence of a complete photonic band gap," Appl. Phys. Lett. **78**, 3388-3390 (2001).
24. H.-Y. Ryu, M. Notomi and Y.-H. Lee, "High-quality-factor and small-mode-volume hexapole modes in photonic-crystal-slab nanocavities," Appl. Phys. Lett. **83**, 4294-4296 (2003).
25. S.-H. Kwon, S.-H. Kim, S.-K. Kim and Y.-H. Lee, "Small, low-loss heterogeneous photonic bandedge laser," Opt. Express **12**, 5356-5361 (2004).
26. A higher-order band edge mode with the wavelength of 1597 nm is observed in Fig. 7(a) (D).
27. S.-K. Kim, G.-H. Kim, S.-H. Kim, S.-B. Kim, I. Kim and Y.-H. Lee, "Loss management using parity-selective barriers for single-mode, single-cell photonic crystal resonators," Appl. Phys. Lett. **88**, 161119 (2006).
28. D. Englund and J. Vuckovic, "A direct analysis of photonic nanostructures," Opt. Express **14**, 3472-3483 (2006).
29. The band edge laser is observed with more increased pumping power. Threshold of the band edge laser is ~650 μW in the PhC cavity of Fig. 6.
30. M.-K. Seo, H.-G. Park, J.-K. Yang, J.-Y. Kim, S.-H. Kim and Y.-H. Lee, "Controlled sub-nanometer tuning of photonic crystal resonator by carbonaceous nano-dots," Opt. Express **16**, 9829-9837 (2008).

1. Introduction

Photonic crystals (PhCs) are efficient structures to manipulate photons at the wavelength-scale [1-10]. One can demonstrate a variety of multifunctional PhC devices with desired optical properties such as high quality (Q) factors [1-3], small mode volumes [4, 5], and a high coupling efficiency with waveguides [6-8]. In particular, low-threshold PhC lasers have attracted much attention as a promising light source in ultracompact nanophotonic integrated circuits and all-optical signal processing [4, 5, 9]. In addition, PhC cavities can constitute a useful toolbox for cavity quantum electrodynamics experiments to demonstrate vacuum Rabi splitting and high-efficiency single photon sources [10, 11].

In order to understand the optical features of the resonant modes found in a PhC cavity, the photonic band structure is typically calculated [12]. Figure 1(a) shows the transverse electric-like (TE-like) band structure of a triangular lattice PhC slab, which is computed by the three-dimensional (3-D) plane-wave expansion method [12]. In this simulation, the air hole radius and the thickness of the slab are $0.3a$ and $0.49a$, respectively, where a is the lattice constant. There exists a photonic band gap for the TE-like modes between the K point of the first band (K1) and the M point of the second band (M2) (Fig. 1(a)). If a cavity is formed by the removal or modification of air holes, the excited cavity modes originate from the band edge points such as K1 or M2 and therefore retain optical properties similar to the corresponding band edge modes [12]. For example, if we remove a single air hole at the center of the triangular lattice PhC slab structure, four different resonant modes (air-band cavity modes) are pulled down into the photonic band gap from the M2 point [13].

#105071 - $15.00 USD Received 9 Dec 2008; revised 20 Jan 2009; accepted 21 Jan 2009; published 27 Jan 2009

Representative electric field intensity profiles of the band edge points, K1 and M2, are shown in Figs. 1(b) and 1(c), respectively. Note that the electric fields at the K1 point are concentrated in the dielectric region (Fig. 1(b)). On the other hand, the electric fields at the M2 point are concentrated in the air region (Fig. 1(c)). The cavity modes pushed up from the K1 point (dielectric-band cavity modes) are particularly interesting because the electric field intensity of the mode will be located in the dielectric region as shown in Fig. 1(b) [14, 15]. Thus, the dielectric-band cavity modes can strongly interact with the gain medium positioned at the dielectric region, e. g., quantum dots. Such strong light-matter interactions are advantageous to the realization of low-threshold lasers and efficient nonlinear optical devices [13-17]. In this study, we investigated optical characteristics of the dielectric-band cavity modes using finite-difference time-domain (FDTD) simulation, and we demonstrated lasing actions from these modes.

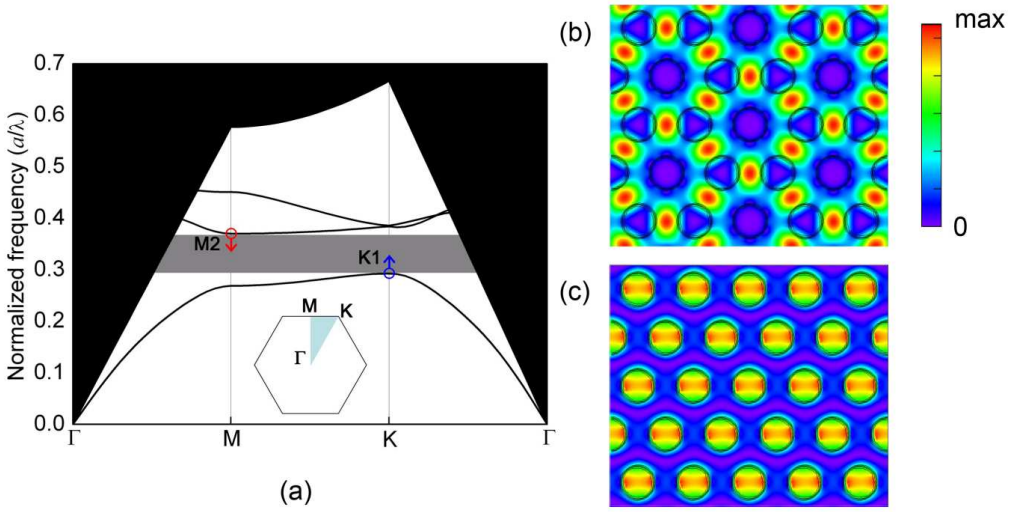

Fig. 1. (a). Calculated TE-like band diagram of the triangular lattice PhC slab structure. The first band edge point (K1) and the second band edge point (M2) are denoted by blue and red circles, respectively. Gray and black regions indicate photonic band gap and leaky modes, respectively. The inset shows the irreducible Brillouin zone of the triangular lattice PhC structure. (b)-(c) The electric field intensity profiles of (b) the K1 band edge mode, and (c) the M2 band edge mode.

2. FDTD simulation: dielectric-band cavity modes versus air-band cavity modes

In order to excite the dielectric-band cavity modes, we employed the modified single-cell PhC cavity shown in Fig. 2(a). The effective index of the cavity was lowered by enlarging air holes around the cavity, and thus the resonant modes were pushed up from the dielectric band (the K1 band edge point) into the photonic band gap [14-16]. One can use a dielectric-band cavity mode to put the electric field maximum in the dielectric region and introduce a single missing air hole in the center [18] to improve the overall electric field overlap with the dielectric region in comparison to the pure graded lattice geometry employed in Refs. [15, 16]. For the effective photon confinement, the radii of the air holes in the first four layers (r_1 to r_4) decrease linearly from the cavity center, but these air holes are larger than the regular one (r_5) (Fig. 2(a)) [19, 20]. The dielectric-band cavity modes can be compared with the conventional air-band cavity modes. By reducing and pushing away the nearest neighbor air holes around the cavity shown in Fig. 2(b), the resonant modes were pulled down from the M2 band edge point [13]. The effective photon confinement can be achieved in the air-band cavity without linearly varying hole radius.

#105071 - $15.00 USD Received 9 Dec 2008; revised 20 Jan 2009; accepted 21 Jan 2009; published 27 Jan 2009

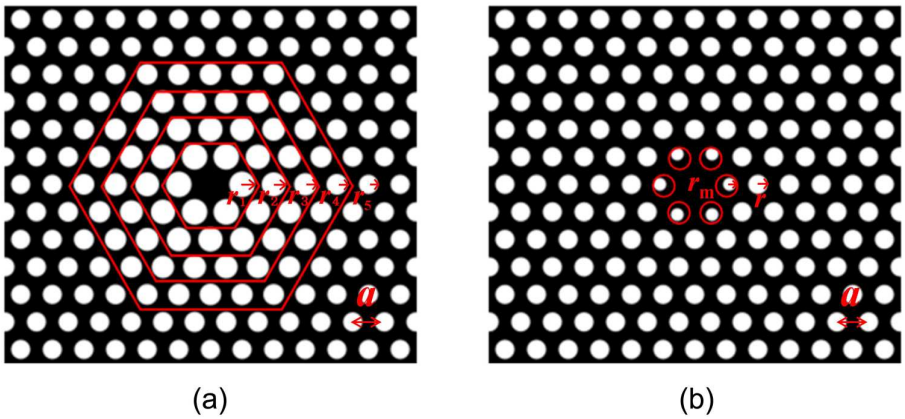

Fig. 2. The modified single-cell PhC cavities for (a) the dielectric-band and (b) the air-band cavity modes. In (a), one missing air hole at the center is surrounded by four layers of air holes with linearly decreasing radii (r_1 to r_4). The air holes with same radii are indicated by the same hexagons. In (b), the six nearest neighbor air holes (r_m) are reduced and pushed away from the cavity center.

To understand the origin of the dielectric-band and the air-band cavity modes, we computed the mode patterns using the 3-D FDTD method [12-15]. First, in the dielectric-band cavity shown in Fig. 2(a), two cavity modes with similar resonant frequencies [21], the hexapole and the monopole modes, were introduced in the bad gap (Fig. 3). In the simulation, the refractive index and the thickness of the slab are set to 3.2 and 210 nm, respectively. For strong confinement of the modes in the cavity, we set lattice constant a, and the radius of the air holes in each layer as follows: a = 430 nm, $r_1 = 0.4a$, $r_2 = 0.375a$, $r_3 = 0.35a$, $r_4 = 0.325a$, and $r_5 = 0.3a$. Note that the electric fields of the hexapole and monopole modes are concentrated in the dielectric region (Figs. 3(a) and 3(b)). Also, the mode profiles in the Fourier space show that the six dominant wavevector components in both modes are localized at the six K points (Figs. 3(c) and 3(d)) [14, 15]. Such field distributions in the real and the Fourier spaces imply that the cavity modes originate from the K1 band edge point, as we expected. In addition, the vertical radiation loss can be qualitatively discussed from the calculated Fourier space intensity profiles [22]. The hexapole mode (Fig. 3(c)) has relatively negligible wavevector components inside the light cone (dotted white circle) compared with the monopole mode (Fig. 3(d)); therefore, the hexapole mode will have a smaller vertical radiation loss than the monopole mode.

#105071 - $15.00 USD Received 9 Dec 2008; revised 20 Jan 2009; accepted 21 Jan 2009; published 27 Jan 2009

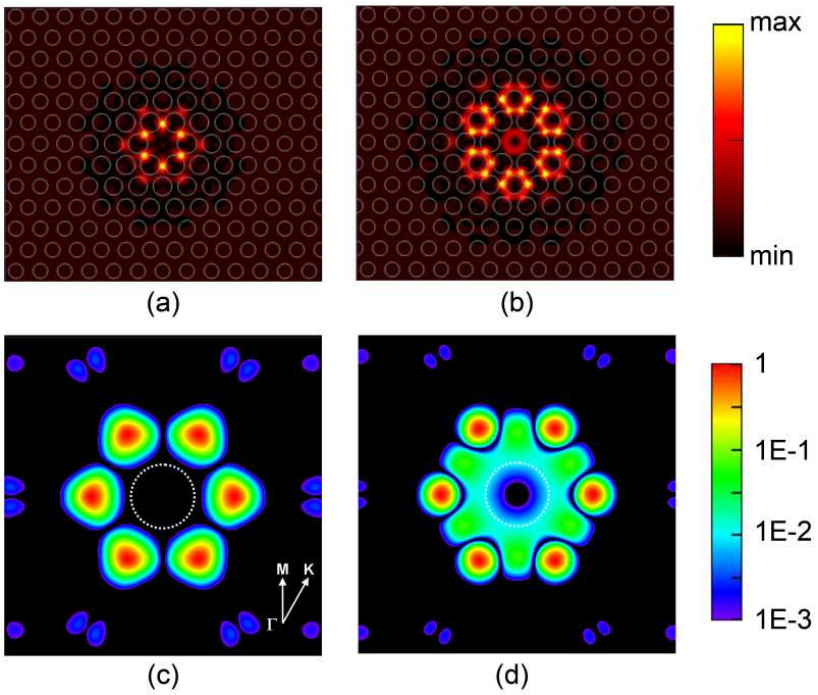

Fig. 3. The calculated mode patterns of the dielectric-band cavity modes. (a)-(b) The electric field intensity profiles (linear-scale) of (a) the hexapole, and (b) the monopole modes. The dielectric confinement factors, defined as the ratio of the energy in the dielectric to the whole energy of the mode, of the hexapole and the monopole modes are computed to 85.0 % and 86.2 %, respectively. (c)-(d) Fourier space intensity profiles (log-scale) of (c) the hexapole and (d) the monopole modes. The dotted white circle represents a light cone. The inset in (c) indicates the directions of wavevectors.

The dielectric-band cavity modes are compared with the air-band cavity modes excited in the modified single-cell cavity of Fig. 2(b). Figures 4(a) and 4(b) show the calculated electric field intensity profiles of the hexapole and the monopole air-band cavity modes [22]. In this simulation, the radii of the reduced (r_m) and regular (r) air holes were set to $0.25a$ and $0.3a$, respectively, where a is the lattice constant. In comparison with the dielectric-band cavity modes in Fig. 3, these air-band cavity modes present distinguishable mode patterns (Figs. 4(a) and 4(b)): the electric fields of the air-band cavity modes are more concentrated in the air region rather than the dielectric region. Thus, the air-band cavity modes originated from the M2 band edge point [14, 15, 22]. One more piece of evidence about the origin of the air-band cavity modes is the Fourier space intensity profile, which is similar to the analysis of the dielectric-band cavity modes. In Figs. 4(c) and 4(d), the dominant wavevector components are clearly distributed at the six M points in Fourier space. In addition, relatively weak intensity of the hexapole mode inside the light cone indicates that the Q value of the hexapole mode will be higher than that of the monopole mode [22]. Moreover, the vertical radiation loss of the dielectric-band cavity modes can be compared with that of the air-band cavity modes through the Fourier space field patterns. In a triangular lattice Brillouin zone, the distance between Γ and K points ($2/3(2\pi/a)$) is greater than the distance between Γ and M points ($1/\sqrt{3}(2\pi/a)$) for a given lattice constant a. This implies that the dominant wavevectors at the K points will be located farther from the light cone than the wavevectors at the M points. Therefore, the dielectric-band cavity modes may have lower vertical radiation loss than the air-band cavity modes. Together with this, the mode delocalization and the multipole-

#105071 - $15.00 USD Received 9 Dec 2008; revised 20 Jan 2009; accepted 21 Jan 2009; published 27 Jan 2009

cancellation of the fields should be considered for more quantitative discussion of high Q factors [23, 24].

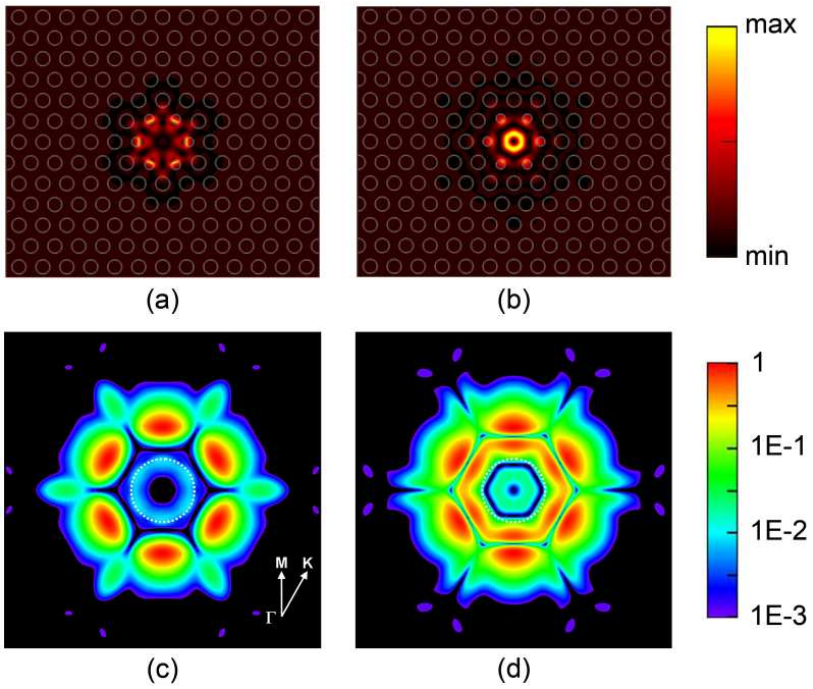

Fig. 4. The calculated mode patterns of the air-band cavity modes. (a)-(b) The electric field intensity profiles (linear-scale) of (a) the hexapole, and (b) the monopole modes. The dielectric confinement factors of the hexapole and the monopole modes are computed to 79.2 % and 83.2 %, respectively. (c)-(d) Fourier space intensity profiles (log-scale) of (c) the hexapole, and (d) the monopole modes. The dotted white circle represents a light cone. The inset in (c) indicates the directions of wavevectors.

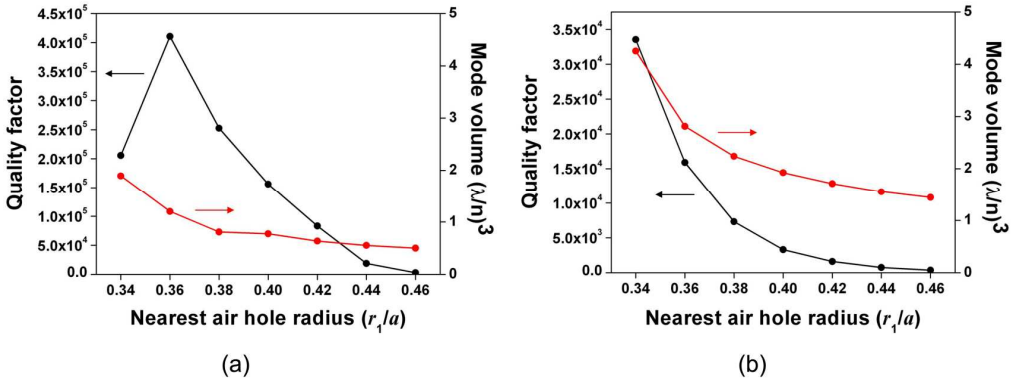

Fig. 5. Calculated Q factors and mode volumes of (a) the hexapole and (b) the monopole dielectric-band cavity modes as a function of the radius of the nearest neighboring holes (r_1) in the PhC cavity of Fig. 2(a). The regular air hole radius r_5 is fixed to $0.3a$. Other air hole radii are determined by the following simple equation (linearly-graded air hole radius): $r_i = r_5 + (5 - i)(r_1 - r_5)/4$, where $i = 1, 2, 3$, and 4.

To investigate the preceding qualitative discussions, we calculated Q factors and mode volumes of the hexapole and the monopole dielectric-band cavity modes as a function of the radius of the nearest neighboring hole (r_1) (Fig. 5). The regular air hole radius (r_5) was fixed

#105071 - $15.00 USD Received 9 Dec 2008; revised 20 Jan 2009; accepted 21 Jan 2009; published 27 Jan 2009

to 0.3a and the other hole radii (r_2 to r_4) in the subsequent layers decreased linearly, as shown in Fig. 2(a). The cavity is surrounded by 30 air holes along the ΓK direction to reduce the horizontal optical loss. The highest Q value of the hexapole mode of 4.1 x 10^5 was computed in our simulation; however, this could be increased if the structural parameters of the cavity were further optimized [23, 24]. Note that the Q factor of the hexapole mode (Fig. 5(a)) is much larger than that of the monopole mode (Fig. 5(b)). This result agrees well with our previous discussion about the vertical radiation loss. In addition, the mode volume of the hexapole mode is almost two times smaller than that of the monopole mode, as already shown in the electric field distributions of Figs. 3(a) and 3(b). One more noticeable point in Fig. 5 is that a high Q factor and small mode volume of the hexapole mode were obtained in a broad range of r_1 (0.34a to 0.40a). On the other hand, the monopole mode is more sensitive to a small variation of the cavity structure. These simulation results are useful to determine the optimized structural parameters for an ultrasmall high Q cavity. Further study is necessary for quantitative comparison of Q factors and mode volumes of the dielectric-band cavity modes with those of the air-band cavity modes.

3. Optical characterization of lasing modes

We fabricated the dielectric-band PhC laser structure, designed as described in the previous section, using typical semiconductor fabrication techniques [5, 13]. Three indium gallium arsenic phosphide (InGaAsP) quantum wells (QWs), whose central emission wavelength is 1.55 μm, were used as an active material, and were embedded in the freestanding InGaAsP slab with a thickness of 210 nm. The PhC patterns were defined by electron beam lithography and transferred into the slab by Ar/Cl_2 chemically-assisted ion beam etching. The sacrificial InP layer beneath the InGaAsP slab was then selectively dissolved with a diluted HCl solution to form a freestanding structure. Figure 6(a) shows the scanning electron microscope (SEM) image of a fabricated PhC structure. The radii of the air holes around the cavity were continuously changed, as we designed in Fig. 2(a). In Fig. 6(b), lattice constant a and the radii of the air holes in each layer are as follows: a = ~430 nm, $r_1 = 0.35a$, $r_2 = 0.33a$, $r_3 = 0.32a$, $r_4 = 0.27a$, and $r_5 = 0.25a$.

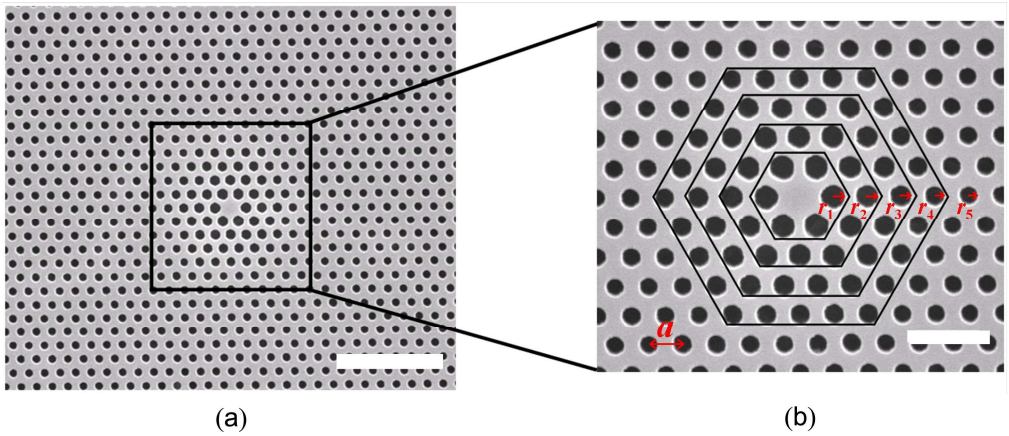

Fig. 6. (a). The SEM image of a fabricated laser structure. The scale bar is 3 μm. (b) The magnified SEM image. The radii of air holes enclosed by each hexagon are denoted by r_1, r_2, r_3, r_4, and r_5. The scale bar is 1 μm.

A photoluminescence (PL) spectroscopy was performed to investigate the optical characteristics of the fabricated PhC cavity structures [5, 13]. The PhC cavities were optically pumped at room temperature by a 980 nm pulsed laser diode (10 ns pulses of 1% duty cycle). A 50x microscope objective lens with a numerical aperture (N.A.) of 0.85 focused the pump

#105071 - $15.00 USD Received 9 Dec 2008; revised 20 Jan 2009; accepted 21 Jan 2009; published 27 Jan 2009

beam to a spot with a diameter of ~3.5 μm. The PL emitted from the PhC cavity was collected by the same lens and fed into either a spectrometer or an infrared (IR) camera. Then, rich lasing actions were observed from the samples with various lattice parameters.

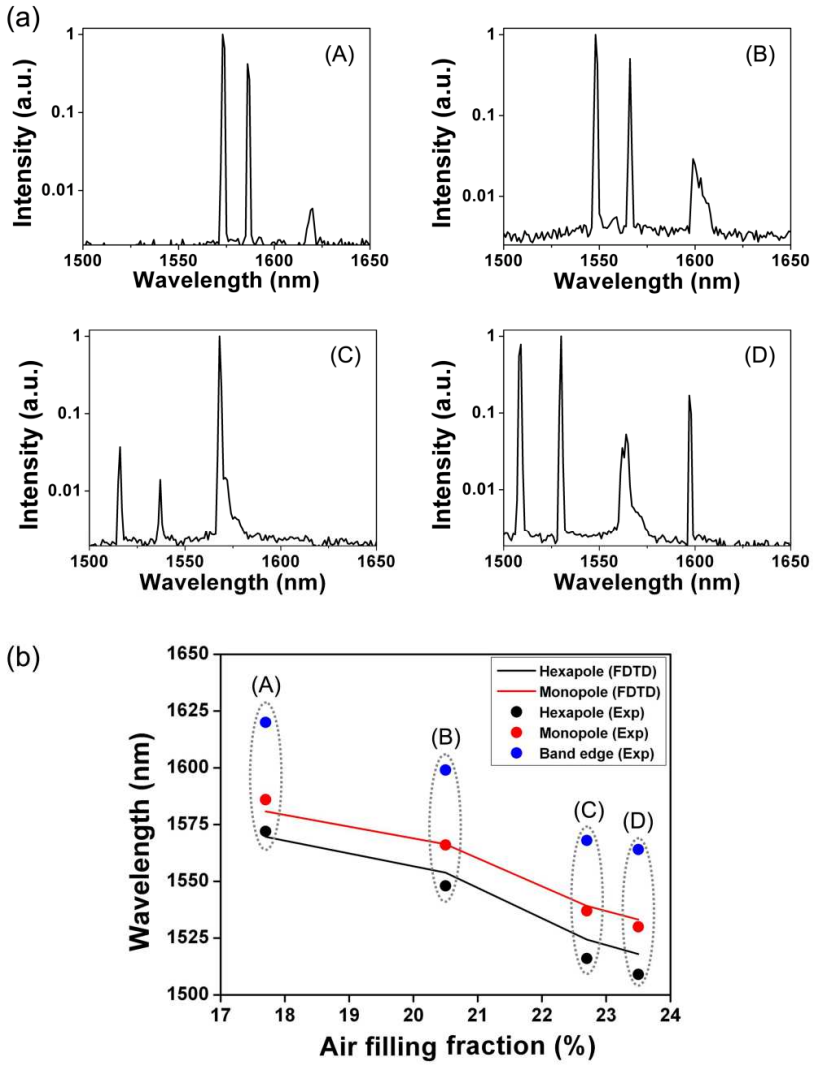

Fig. 7. (a). Typical above-threshold PL spectra (log-scale) measured in four different samples (A) to (D). Air hole sizes increase from samples (A) to (D). (b) The resonant wavelength of each mode is plotted as a function of air filling fraction. The resonances in each sample are grouped by the gray dotted line. The measured resonances are indicated by dots and the calculated resonances by lines. The black, red, and blue dots are the resonant wavelengths of the hexapole, monopole and band edge modes, respectively.

Figure 7(a) shows above-threshold PL spectra measured in four PhC cavity structures, (A) to (D), which have different air hole sizes but a fixed lattice constant of ~430 nm. As the air hole sizes increase from the samples (A) to (D), the wavelengths of the multimode resonant peaks blue-shift. In Fig. 7(b), we plotted the wavelengths of these measured peaks as a function of air filling fraction, defined as the ratio of the air to the entire area including the cavity region in the fabricated PhC structure of Fig. 6(a). In this graph, note that the spectral spacing between the two modes with short wavelengths (black and red dots) is quite small. On the other hand, the third one (blue dot) is relatively distant from the two modes in all the

#105071 - $15.00 USD Received 9 Dec 2008; revised 20 Jan 2009; accepted 21 Jan 2009; published 27 Jan 2009

samples. Considering the previous FDTD simulations performed in the dielectric-band PhC cavity (Section 2), the first two modes with similar wavelengths (black and red dots) are supposed to be the hexapole and the monopole modes. On the other hand, the third mode (blue dot) exhibited distinguishable characteristics from the other two cavity modes such as a spectral position relatively far from the other modes, and a broad peak shape (Fig. 7(a)); hence, this would be the band edge resonant mode [25, 26].

The observed mode images strongly support this spectral mode identification [13, 27]. Figures 8(a), 8(b), and 8(c) show typical lasing mode images of the black, red, and blue dots in Fig. 7(b), respectively, captured by the IR camera. To observe only a single-lasing mode in each image, we optimized the pumping power and position, and also placed the bandpass filters with the central wavelengths corresponding to the respective lasing wavelengths and full width at half-maximum (FWHM) of 20 nm in front of the IR camera. In Figs. 8(a) and 8(b), the lasing modes are strongly confined in the central cavity region, and thus correspond to the dielectric-band cavity modes (the hexapole mode and the monopole mode) [13, 27]. In addition, since the mode volume of the monopole mode is clearly larger than that of the hexapole mode (calculated as shown in Fig. 5), the smaller lasing mode will be the hexapole mode (Fig. 8(a)) and the slightly larger mode will be the monopole mode (Fig. 8(b)). Furthermore, the FDTD simulation based on the actual fabricated structural parameters, to be introduced in the next section in detail [13, 28], agrees well with such analysis (see the solid lines in Fig. 7(b)). Therefore, the black and red dots in Fig. 7(b) represent the hexapole and the monopole lasing modes, respectively. On the other hand, the band edge mode of Fig. 8(c) is obviously distinguishable from the other two cavity modes. The volume of the mode broadly distributed outside the cavity region is extraordinarily large relative to the cavity modes [25]. The band edge lasing condition is satisfied in the outer region of the cavity which consists of regular air holes of radius r_5. Consequently, we can successfully identify all resonant modes appearing in the dielectric-band cavity structure by the measurement of PL spectra and lasing mode images.

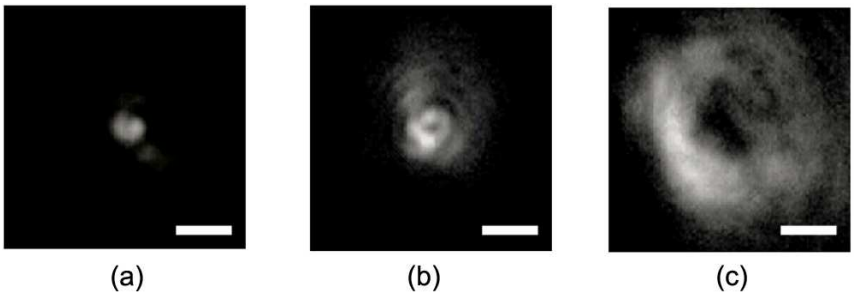

Fig. 8. Lasing mode images of (a) hexapole, (b) monopole, and (c) band edge modes, captured by an IR camera. All scale bars are 5 μm. Only a single-lasing mode is observed in each image. The pumping powers and the central wavelengths of the bandpass filters are (a) 426 μW and 1509 nm, (b) 527 μW and 1530 nm, and (c) 850 μW and 1564 nm. In (c), the effective transparent region is increased due to the relatively high pumping power.

To further investigate the optical properties of the lasing modes, we measured PL intensities as a function of the pump power. Figure 9(a) shows PL spectra measured at the pump powers of 426 μW and 527 μW in the fabricated PhC structure shown in Fig. 6. At a low pump power of less than ~450 μW, a single-lasing peak with a wavelength of 1509 nm corresponding to the hexapole mode was observed. When the pump power was increased (~450-600 μW), one more sharp peak, the monopole-mode lasing, appeared at 1530 nm. In Figs. 9(b) and 9(c), these peak intensities of the hexapole-mode and the monopole-mode lasers are plotted as a function of the incident pump power. In both plots, superlinear increases are clearly observed, and the lasing threshold powers are ~340 μW and ~450 μW for the

#105071 - $15.00 USD Received 9 Dec 2008; revised 20 Jan 2009; accepted 21 Jan 2009; published 27 Jan 2009

hexapole-mode and the monopole-mode lasers, respectively [29]. Note that the threshold of the hexapole-mode laser is lower than that of the monopole-mode laser due to the higher Q and smaller mode volume of the hexapole mode (Fig. 5) [5, 13]. As a result, PL spectroscopy demonstrates that a single-mode lasing action can be achieved at low incident pump power (~340-450 μW); however, it is not straightforward to obtain single-mode lasing even at higher pump power due to the close spectral spacing between the hexapole and the monopole modes. Additional structural modification to selectively increase an optical loss of an undesired mode will be required for single-mode lasing at higher pump power [27, 30].

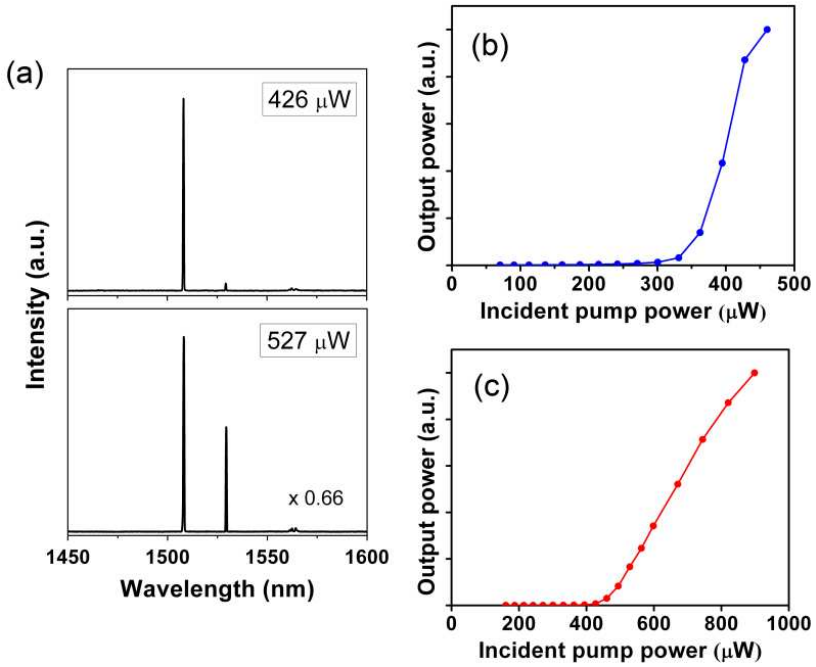

Fig. 9. (a). PL spectra at different incident pump powers of 426 μW (top) and 527 μW (bottom). Only the hexapole-mode lasing is observed at 426 μW; however, the monopole-mode lasing peak is additionally observed at 527 μW. (b)-(c) Lasing peak intensity vs. incident pump power for (b) the hexapole mode, and (c) the monopole mode. Threshold pump powers of the hexapole-mode and the monopole-mode lasers are ~340 μW and ~450 μW, respectively.

4. Comparison of measurements with numerical simulations

So far, we have analyzed the measured optical properties of the lasing modes in the dielectric-band PhC cavity by comparing them with the 3-D FDTD simulation results of Section 2. In fact, if all imperfections in fabrication are considered in the simulation, such comparison can undoubtedly be reliable and accurate. The numerical structural input data in this simulation are directly obtained from the SEM images taken from the fabricated samples [13, 28]. Figure 10(a) shows the cavity region of the PhC structure in the FDTD computation domain that is transformed from the SEM image of Fig. 6(a). The resolution of the SEM image in Fig. 6(a) is 25 nm and the sub-grid size in our FDTD calculation is 2.5 nm. Thus, the roughness of the structure in the SEM image is fully considered in FDTD simulation. Then, the FDTD simulation demonstrates that two cavity modes, the hexapole and the monopole modes, are successfully excited in the PhC cavity even though we take into consideration all actual imperfections (Fig. 10(b)).

To better understand the spectral mode identification performed in Fig. 7, we used this powerful FDTD simulation method for samples (A) to (D) [4]. The hexapole and the monopole modes were excited in all the fabricated samples as shown in Fig. 10(b). The

#105071 - $15.00 USD Received 9 Dec 2008; revised 20 Jan 2009; accepted 21 Jan 2009; published 27 Jan 2009

calculated wavelengths of the cavity modes are plotted in Fig. 7(b) (solid lines) together with the measured wavelengths (dot symbols). Black and red lines are the hexapole and the monopole modes in FDTD, respectively. Note that the two cavity modes closely located in the cavity of Fig. 3, the hexapole and the monopole modes, are now further split due to the structural imperfections considered in the simulation. It is surprising that the simulation results agreed well with the measurements. Therefore, the actual lasing modes operate in the hexapole and monopole modes (Fig. 7), as clearly shown by comparison of the measurements with the computations based on actual fabricated structural parameters.

Next, using this FDTD simulation, we further investigated optical properties of the two cavity modes including actual mode volumes and Q factors (Fig. 10(b)) [5, 13]. In the fabricated PhC cavity shown in Fig. 6, the mode volumes of the hexapole and the monopole modes were calculated to be 1.09 $(\lambda/n)^3$ and 2.27 $(\lambda/n)^3$, respectively, where λ is the resonant wavelength of the corresponding mode and n is the refractive index of the slab. These values are similar to the results shown in Fig. 5. On the other hand, Q factors of the hexapole and the monopole modes were calculated to be 4900 and 4300, respectively. The fact that the calculated Q factors for structures including the fabrication imperfections are significantly smaller than those of the ideal structure can be understood by the vertical radiation loss mechanism [28]. When the photons in a cavity are scattered by the structure imperfections, they are redirected upward and lost out of the cavity. These realistic Q factors and mode volumes are particularly meaningful for comparison of the measured thresholds. It is straightforward that the threshold of the hexapole-mode laser with a higher Q and smaller mode volume is lower than that of the monopole-mode laser (Figs. 9(b) and 9(c)). Hence, the FDTD simulation based on the actual fabricated structural parameters is a promising tool to analyze and understand the experimentally measured optical properties.

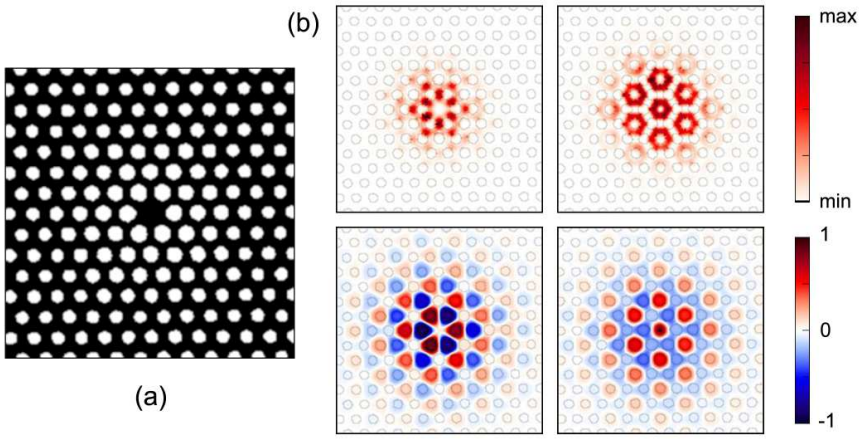

Fig. 10. (a). Cavity structure transformed from the SEM image of the fabricated sample in Fig. 6. (b) The electric field intensity profiles (top) and H_z-field profiles (bottom) of the hexapole (left) and the monopole modes (right). The mode profiles of each mode agreed well with the profiles of the corresponding ideal structure.

5. Conclusion

We investigated the dielectric-band and air-band cavity modes in two properly designed modified single-cell PhC cavities. From the field intensity distributions of each cavity mode computed in the real and the Fourier spaces using FDTD simulation, we understood that the dielectric-band and air-band cavity modes originated from the K1 and M2 band edge points, respectively. The Q factor and mode volume were computed for the dielectric-band cavity modes, and the structural parameters for high Q and small mode volume were found. In an experiment, multimode lasing actions, the hexapole-mode and the monopole-mode lasers,

#105071 - $15.00 USD Received 9 Dec 2008; revised 20 Jan 2009; accepted 21 Jan 2009; published 27 Jan 2009

were observed with respective low thresholds of ~340 μW and ~450 μW in the PhC cavity that effectively confined the dielectric-band cavity modes. These lasing modes were successfully identified by the measurements of the PL spectra and the mode images. In addition, FDTD simulation based on the actual fabricated structural parameters showed that the measured optical properties agreed well with the simulation results. Dielectric-band cavity modes that can strongly interact with the gain medium positioned at the dielectric region will be useful in the demonstration of low threshold lasers and efficient nonlinear optical devices.

Acknowledgment

This work was supported by a Korea Research Foundation Grant funded by the Korean Government (KRF-2008-331-C00118).

#105071 - $15.00 USD Received 9 Dec 2008; revised 20 Jan 2009; accepted 21 Jan 2009; published 27 Jan 2009